Linear and nonlinear poroelastic analysis of swelling and drying behavior of gelatin-based hydrogels

Si Chen , Rui Huang , Krishnaswamy Ravi-Chandar

PII: S0020-7683(20)30105-0
DOI: https://doi.org/10.1016/j.ijsolstr.2020.03.017
Reference: SAS 10655

To appear in: *International Journal of Solids and Structures*

Received date: 9 December 2019
Revised date: 24 February 2020
Accepted date: 19 March 2020

Please cite this article as: Si Chen , Rui Huang , Krishnaswamy Ravi-Chandar , Linear and nonlinear poroelastic analysis of swelling and drying behavior of gelatin-based hydrogels, *International Journal of Solids and Structures* (2020), doi: https://doi.org/10.1016/j.ijsolstr.2020.03.017

Linear and nonlinear poroelastic analysis of swelling and drying behavior of gelatin-based hydrogels

Si Chen, Rui Huang and Krishnaswamy Ravi-Chandar

Center for Mechanics of Solids, Structures and Materials
Department of Aerospace Engineering and Engineering Mechanics
The University of Texas at Austin
Austin, TX 78712-1221
ravi@utexas.edu

Abstract

The swelling and drying behavior of a gelatin-glycerol-water hydrogel are examined experimentally for different compositions and different environmental conditions. Significant asymmetry in the swelling and drying kinetics is observed from these measurements. The early time measurements are interpreted first within the context of a linear poroelastic theory, but a fully nonlinear Flory-Rehner theory is required in order to capture the long time behavior. Comparison of the experimental measurements with simulations based on both the linear and nonlinear constitutive models yields a consistent calibration of the material parameters of the models.

1. Introduction

Hydrogels are soft materials that consist of a polymer network embedded in a solvent that is predominantly water. The ability of hydrogels to absorb and retain a large amount of water without disintegrating and still maintaining a solid-like phase makes hydrogels appealing in a wide range of applications in various fields, such as contact lenses, drug delivery, tissue engineering, and agriculture industry (Ullah 2015). In many of these applications, it is necessary to consider the coupling of diffusion of the solvent through the network and deformation of the network in assessing their response to changes in the chemical and mechanical environment; this is accomplished within the theory of poroelastcity. The theory of linear poroelasticity was developed based on the ideas of Gibbs (1878), Biot (1941) and others; Biot's theory of linear poroelasticity, combining linear elasticity of the solid matrix and Darcy's Law of flow, is often used to describe hydrogels as fluid-saturated porous media (Yoon et al 2010). Nonlinear models have also been presented (see Flory, 1942; Huggins, 1941, Hong et al. 2008, 2009; Chester and Anand, 2010; Bouklas and Huang, 2012; Bouklas et al. 2015 and others) for coupling large deformation and solvent diffusion in the poroelastic material. In this work, we will begin with the linear theory of poroelasticity followed by a nonlinear theory in comparison with experiments.

There are two types of hydrogels – thermo-reversible physical gels and irreversible chemical gels (see te Nijenhuis, 1997). Both are formed by dissolving the network forming molecules in a solvent to form a solution; when cooled below a critical temperature, a transition to a solid-like structure occurs; the resulting structure can sustain a shear stress, facilitated by the formation of a percolating network of bonds spanning the system. In the case of the physical gels, these bonds

arise due to entanglements, crystallite formation, helix formation, phase separation or hydrogen bonds; the network formed by these mechanisms are thermally reversible thereby endowing the *gel* with this property. In the case of chemical gels, the bonds are typically associated with reactions between monomers to form a network polymer or simply cross-linking as in vulcanization reactions in rubber; these bonds are usually not thermally reversible. The gelatin based hydrogel considered in this work is usually formed into a physical gel by mixing the protein collagen in a mixture of glycerol and water. The network structure is formed as the denatured coiled collagen in the gelatin reforms its triple-helical structure upon cooling below the critical temperature and acts as "crosslinks"; a schematic of the formation of the network is shown in Figure 1 (Harrington and Rao, 1970). It is also possible to generate a collagen-based chemical gel by crosslinking using glutaraldehyde (Lee and Mooney, 2001); this type of gel is used in numerous biological applications, but is not considered here.

Glycerol is not a good solvent for the collagen, but the mixture of glycerol and water is a marginal solvent (Tice and Moore, 1950, Sanwlani et al 2011); Sanwlani et al also indicate that very few of the glycerol molecules attach to the gelatin chains. Therefore, glycerol does not participate directly in the gelation process, but occupies volume, and provides shear resistance that impacts the viscosity of the resulting gel. Baumberger et al (2006) used this gelatin based gel in a water-glycerol mixture to influence the viscous response and studied the fracture behavior of the resulting gel. Moreover, glycerol delays bacterial growth on the gelatin so that long time experiments (more than five days) such as swelling/drying could be performed without affecting the gelatin-based gel.

There are several types of mechanical tests designed to extract linear poroelastic properties, like the indentation (Chan et al 2011) and compression (Cai et al 2010) tests. We note that most of tests are performed with the specimen fully immersed in the solvent, while in practical applications, the hydrogel can be exposed to the solvent only through the humidity of the ambient air. For example in sol-gel processing, such an approach is used to remove the solvent. The key difference arises from the fact that while the hydrogel immersed in the water always swells, the hydrogel kept in low-humidity air could lose water; such drying effects are important in many applications. Hence, in this paper, we examine the poroelastic behavior both under swelling and drying conditions.

2. Materials and Methods

2.1. Specimen preparation

The gelatin-based hydrogel was prepared by dissolving Fisher gelatin type A (G8-500, derived from porcine collagen) into a solvent with the weight fraction of 15% of gelatin and 85% of a water-glycerol mixture with the specific mixtures of composition A and B listed in Table 1. We choose two different compositions to probe the effect of initial chemical potential on the swelling/drying response; complete characterization requires more compositions to be tested. The solution was heated to a temperature of 80 °C with continuous stirring until the gelatin powder dissolved completely in the glycerol-water solution. It was then placed in a vacuum oven at 50 °C and evacuated at less than 6.897 kPa for about thirty minutes to remove smaller air bubbles. The solution was then poured into a mold to form suitable specimens for the different

experiments and allowed to cool to room temperature of ~25 °C. Fully transparent gels were formed, with bubbles, if present, below sizes where their presence would scatter light. The specimens were removed from the mold, and swelling/drying tests were performed 24 hours after preparation.

2.2. Experimental methods

For the drying/swelling experiments, parallelepipedic specimens that were 30 mm x 10 mm x 3 mm were fabricated as indicated above. All the tests were performed at room temperature (~25 °C) in humidity controlled chambers with the relative humidity (RH) ranging from 5% to 100%. We note that there are two solvents in this gel – glycerol and water. Controlling the humidity influences the chemical potential for water and results in either drying or swelling depending on the chemical potential difference between the specimen and the environment. Since the hydrogels are quite weak, the specimens were fabricated with integral gripping fixtures as illustrated in Figure 2a. The front surface of the specimen was decorated by scattering a fine dust of titanium dioxide particles that adhere to the surface of the specimen; this pattern was viewed with a dark background and the resulting pattern shown in Figure 2b was used in the calculation, through digital image correlation (DIC), of the principal in-plane strains on the surface as a function of time, enabling tracking of the drying/swelling deformation of the gel. For the drying and swelling experiments, the specimens mounted on the grips were suspended freely from the top of the environmental chamber at a specified humidity level; this corresponds to free drying or free swelling conditions. The stress due to self-weight of the gel is only on the order of a few Pa and is neglected in the analysis. A Zipscope video microscope was used to acquire images of the front surface at ten minutes time intervals for about 160 to 180 hours. The images were then processed using the ARAMIS DIC software to extract the vertical and horizontal strain components, ε_y and ε_x; in order to decrease the noise and improve the precision of the strain measurements, the strains were averaged over a rectangular patch of approximately 9 mm by 27 mm, avoiding the edges of the specimen where the DIC measurements are typically more noisy. Specimens of both compositions A and B were placed in the chambers at around 15% RH to dry, at around 100% RH to swell, and at around 73% for composition A and 85% for composition B to maintain equilibrium without swelling or drying.

3. Results

The time variation of the average strain ε_y from the tests is shown in Figure 3; the time variation of ε_x is similar and therefore not shown. There are six sets of curves in this figure, corresponding to two compositions (A and B), and three conditions of humidity (15%, 73% and 100% for composition A; 15%, 85% and 100% for composition B); the responses appear to be grouped similarly. It should be remarked that the scatter seen in these measurements for each group of specimens arises from small differences in the glycerol-water mixture or weight of gelatin that are introduced during manufacturing of multiple specimens. Clearly, for both compositions, the dry/humid environment results in shrinking/swelling of the gel by ejecting water to or absorbing water from the environment. Composition B, with a higher initial water content, has a higher drying strain and a lower swelling strain when compared to Composition A,

with a lower initial water content. The diffusive nature of the strain evolution is evident from these measurements. Asymmetry between drying and swelling is also noticeable from these results.

Interpretation of the data from these drying and swelling experiments requires an underlying transient theory based, at a minimum, on poroelasticity. We will consider first a linear poroelasticity theory and subsequently a nonlinear theory for a consistent calibration of the material parameters. The effect of viscoelasticity is ignored in the present study.

4. Linear poroelasticity

The theory of linear poroelasticity was developed based on ideas presented by Gibbs (1878), Biot (1941) and others; this was presented in the context of a continuum thermodynamics framework by Anand (2015). We will follow the notation of the latter to summarize the equations of linear poroelasticity first, and then consider its numerical solution to compare with the drying and swelling experiments.

4.1. Balance Laws

Let $\mathbf{u}(\mathbf{x},t)$ be the displacement field, $\boldsymbol{\varepsilon}(\mathbf{x},t)=\left(\nabla\mathbf{u}+(\nabla\mathbf{u})^T\right)/2$ the corresponding infinitesimal strain tensor, $\boldsymbol{\sigma}(\mathbf{x},t)$ the stress field, and $\mathbf{b}(\mathbf{x},t)$ the body force field per unit volume. Balance of linear momentum requires that

$$\nabla\cdot\boldsymbol{\sigma}+\mathbf{b}=\mathbf{0} \tag{1}$$

The relationship between $\boldsymbol{\sigma}(\mathbf{x},t)$ and $\boldsymbol{\varepsilon}(\mathbf{x},t)$ needs to be specified, but this has to be coupled with the solvent effects as summarized below.

Let c_0 be the number of solvent molecules per unit volume in the gel as manufactured. Depending on the ambient environment in which the gel is placed, this may increase (upon swelling) or decrease (upon drying) and so we set $c(\mathbf{x},t)$ to be the time-dependent concentration field. This brings a fluid balance equation into the picture: the rate of flow of the solvent through the boundaries of a volume must balance out the rate of change of concentration of the solvent within the volume. Therefore,

$$\int_{\Omega}\dot{c}\,dV=-\int_{\partial\Omega}\mathbf{j}\cdot\mathbf{n}\,dV \tag{2}$$

where the super dot indicates differentiation with respect to time, $\mathbf{j}(\mathbf{x},t)$ is the solvent flux (number of solvent molecules diffusing per unit area of the boundary per unit time), and $\mathbf{n}(\mathbf{x},t)$ is the outward unit normal to the surface $\partial\Omega$ bounding the volume Ω. Using the divergence theorem, the flux balance can be rewritten in the differential form as:

$$\dot{c}=-\nabla\cdot\mathbf{j} \tag{3}$$

The fluid flux is assumed to be governed by Fick's law:

$$\mathbf{j} = -m\nabla\mu \tag{4}$$

where m is the diffusion coefficient, and μ is the chemical potential of the solvent that is defined as the derivative of the free energy with respect to the solvent concentration in the nonlinear theory (see later Eq.(31)) and is consistently linearized (see Bouklas and Huang, 2012, and Anand, 2015).

4.2. Constitutive Equations for Linear Poroelasticity

In classical linear poroelasticity (Biot 1941), the constitutive relation is written as

$$\boldsymbol{\sigma} = 2G\boldsymbol{\varepsilon} + \lambda^{dr} tr(\boldsymbol{\varepsilon})\mathbf{1} + \frac{\beta}{\Lambda}(\mu - \mu_0)\mathbf{1} \tag{5}$$

$$c = c_0 - \frac{\beta}{\Lambda} tr(\boldsymbol{\varepsilon}) + \frac{1}{\Lambda}(\mu - \mu_0) \tag{6}$$

where G is the shear modulus, λ^{dr} is called the "drained" Lame modulus, and β and Λ are poroelastic constants, related to the Biot modulus M, Biot coefficient α and solvent molecular volume, ν, as follows:

$$\beta = -\alpha M\nu, \ \Lambda = M\nu^2 \tag{7}$$

The Biot modulus M is related to the undrained bulk modulus, K, and drained bulk modulus, K^{dr} as follows:

$$M = K - K^{dr} \tag{8}$$

In formulating and solving boundary value problems, it is often convenient to consider the fluid balance in terms of the chemical potential rather than concentration. The concentration $c(\mathbf{x},t)$ can be eliminated between Eqs. (3), (4) and (6), in favor of the chemical potential μ; the resulting diffusion equation is:

$$\frac{1}{\Lambda}\dot{\mu} = \frac{\beta}{\Lambda} tr(\dot{\boldsymbol{\varepsilon}}) + m\nabla^2\mu \tag{9}$$

The first term on the right hand side represents the rate of dilation of the gel and plays an important role in the diffusion of the solvent. Therefore the governing equations for stress in Eq. (1) are coupled to the diffusion equation for chemical potential in Eq. (9) through the constitutive relations in Eq. (5). While the coupling is of interest for general poroelastic materials, for the hydrogels in particular, we may assume that volume change occurs only through change in the solvent concentration whereas the solvent molecules are incompressible with a constant molecular volume *v* (Hong et al. 2009); this will simplify the equations. This limit is obtained by taking $\alpha \to 1$ and $M \to \infty$ so that $\Lambda \to \infty$ and

$$\frac{\beta}{\Lambda} \to -\frac{1}{\nu} \tag{10}$$

Then, the last term of Eq. (6) vanishes, which indicates that the volume change arises simply from uptake or loss of the solvent:

$$\nu\left(c-c_0\right)=\ \mathrm{tr}\left(\boldsymbol{\varepsilon}\right) \tag{11}$$

Eq. (9) can now be reduced to the following form:

$$\mathrm{tr}\left(\dot{\boldsymbol{\varepsilon}}\right)=m\nu\nabla^2\mu \tag{12}$$

This can be recast in the form of the standard diffusion equation by substituting Eq. (5) into Eq. (1), considering zero body force, and eliminating $\nabla\mu$:

$$\mathrm{tr}\left(\dot{\boldsymbol{\varepsilon}}\right)=D^*\nabla^2\mathrm{tr}\left(\boldsymbol{\varepsilon}\right) \tag{13}$$

where $D^*=m\nu^2\left(2G+\lambda^{dr}\right)$ is the effective diffusivity. In addition, we need to examine the boundary conditions, both for the elastic fields and the chemical potential as discussed in the following sections.

4.3. Nondimensional Form of the Governing Equations

Prior to consideration of numerical simulations, attention is paid to the material properties and normalization of the governing equations. From the constitutive relations described above, it is clear that four independent material parameters are involved, two for isotropic linear elasticity, $\left(G,\lambda^{dr}\right)$, one for the solvent molecule, ν, and one for the solvent diffusion, m or D^*. The physical parameters of poroelasticity can then be suitably normalized as follows:

$$\begin{aligned}
&\bar{\mathbf{x}}\rightarrow\frac{\mathbf{x}}{l}\quad \bar{t}\rightarrow\frac{tm\nu k_BT}{l^2}\\
&\bar{\boldsymbol{\sigma}}\rightarrow\frac{\boldsymbol{\sigma}}{G},\quad \bar{\mathbf{b}}\rightarrow\frac{\mathbf{b}l}{G},\quad \bar{\lambda}\rightarrow\frac{\lambda^{dr}}{G},\\
&\bar{\mu}\rightarrow\frac{\mu}{k_BT},\ \bar{A}=\frac{k_BT}{G\nu}
\end{aligned} \tag{14}$$

where l is a length associated with the smallest specimen dimension, k_B Boltzmann constant and T the temperature. The governing equations can then be written in the following dimensionless form for use in computations (with the bars removed):

$$\begin{aligned}
&\nabla\cdot\boldsymbol{\sigma}+\mathbf{b}=\mathbf{0}\\
&\mathrm{tr}\left(\dot{\boldsymbol{\varepsilon}}\right)=\nabla^2\mu\\
&\boldsymbol{\sigma}=2\boldsymbol{\varepsilon}+\lambda\left[\mathrm{tr}\left(\boldsymbol{\varepsilon}\right)\right]\mathbf{1}-A\left(\mu-\mu_0\right)\mathbf{1}
\end{aligned} \tag{15}$$

Note that we have normalized time by $\tau_1=l^2/\left(m\nu k_BT\right)$, but could also have used the effective diffusivity, D^*, and describe the characteristic time as $\tau_2=l^2/D^*$; the two time scales are related easily: $\tau_2=\tau_1\left(A/\lambda\right)$, assuming $\lambda\gg2$, which we verify from later parameter extraction

results. The coupled stress-diffusion equations are solved using a finite element method, implemented in the software FEniCS as described in Section 4.5. These equations contain two dimensionless parameters (λ, A), while the molecular volume of the solvent ν and the diffusion coefficient m are embedded in the normalized time. Determination of these parameters requires experimental measurements; we will use measurements of the strains in swelling/drying experiments to determine some of these material parameters. Calibration of these parameters is discussed further in Section 4.7.

4.4. Initial and Boundary Conditions

The initial conditions for displacement field and chemical potential field are described as follows:

$$\left.\begin{aligned}\mathbf{u}(\mathbf{x},0)&=\mathbf{u}_0(\mathbf{x})\\ \mu(\mathbf{x},0)&=\mu_0(\mathbf{x})\end{aligned}\right\} \quad \text{on} \quad \Omega \tag{16}$$

where $\mathbf{u}_0(\mathbf{x})$, $\mu_0(\mathbf{x})$ are prescribed functions. The boundary conditions for the elastic field are the usual displacement or traction boundary conditions:

$$\begin{aligned}&\mathbf{u}(\mathbf{x},t)=\mathbf{u}_t(\mathbf{x},t) \quad \text{on} \quad \partial\Omega_u\\ &\mathbf{t}(\mathbf{x},t)=\boldsymbol{\sigma}\mathbf{n}=\mathbf{t}_t(\mathbf{x},t) \quad \text{on} \quad \partial\Omega_t\end{aligned} \tag{17}$$

where $\partial\Omega_u$ and $\partial\Omega_t$ are the displacement and traction boundary segments, $\mathbf{n}$ is the unit outward normal to $\partial\Omega_t$, and $\mathbf{u}_t(\mathbf{x},t)$, $\mathbf{t}_t(\mathbf{x},t)$ are prescribed functions. Similarly, for the chemical potential, we may have Dirichlet or Neumann boundary conditions:

$$\begin{aligned}&\mu(\mathbf{x},t)=\mu_t(\mathbf{x},t) \quad \text{on} \quad \partial\Omega_D\\ &\nabla\mu(\mathbf{x},t)\cdot\mathbf{n}=g_t(\mathbf{x},t) \quad \text{on} \quad \partial\Omega_N\end{aligned} \tag{18}$$

where $\partial\Omega_D$ and $\partial\Omega_N$ are the Dirichlet and Neumann boundary segments, and $\mu_t(\mathbf{x},t)$, $g_t(\mathbf{x},t)$ are prescribed functions. However, the real boundary condition for the chemical potential is likely to be more complex; because the drying/swelling experiments considered in this work were performed in an environment with humid air, the solvent molecules have to diffuse through the gel, evaporate on the surface, and convect into the air. Hence it would appear that neither the chemical potential, nor its normal flux is being controlled; considerations of this type of boundary conditions were discussed in relation to drying of gels by de Gennes (2002). This is also analogous to boundary conditions used in heat transfer or the traction-separation law in modeling cohesive fracture of solids. One way of handling this situation is to introduce a general Robin boundary condition at all boundaries where the gel is in contact with the external environment, by taking the normal flux to be some function of the chemical potential difference across the boundary. Thus,

$$\nabla\mu\cdot\mathbf{n}=f(\mu-\mu_\infty) \quad \text{on} \quad \partial\Omega_R \tag{19}$$

where μ_∞ is the chemical potential in the environment, μ is the chemical potential in the gel, and $f(\mu-\mu_\infty)$ is some arbitrary function, yet unspecified. In the absence of detailed modeling of this boundary condition, we assume a simple form, $f(\mu-\mu_\infty)=-\alpha_R(\mu-\mu_\infty)$ and attempt to identify the parameter α_R. Note that the Robin boundary condition tends to a Dirichlet condition as $\alpha_R\to\infty$ and a Neumann condition as $\alpha_R\to 0$.

4.5. The Weak Form

We write the weak-form of the governing equations by considering test functions $\mathbf{v}$ and q for the displacement vector field and chemical potential scalar field, respectively. Multiplying the mechanical equilibrium equations by the test function $\mathbf{v}$ and integrating over the volume, and using the divergence theorem yields

$$\int_\Omega (\boldsymbol{\sigma}:\nabla\mathbf{v})\,dV=\int_\Omega (\mathbf{b}\cdot\mathbf{v})\,dV+\int_{\partial\Omega_t}(\mathbf{t}\cdot\mathbf{v})\,dS \tag{20}$$

Similarly, multiplying the diffusion equation by the test function q yields

$$\int_\Omega (\nabla\mu)\cdot(\nabla q)\,dV+\int_\Omega \mathrm{tr}(\dot{\boldsymbol{\varepsilon}})\,q\,dV=\int_{\partial\Omega_N}(\nabla\mu\cdot\mathbf{n})\,q\,dS \tag{21}$$

An implicit backward Euler scheme can be used for the time integration of Eq. (21), to yield an incremental formulation as

$$\int_\Omega \left[dt(\nabla\mu)\cdot(\nabla q)+(\nabla\cdot\mathbf{u})\,q\right]dV=\int_\Omega (\nabla\cdot\mathbf{u}^t)\,q\,dV+dt\int_{\partial\Omega_R}(\nabla\mu\cdot\mathbf{n})\,q\,dS \tag{22}$$

where terms without a superscript belong to time $t+dt$ and the terms from the previous time step at t are indicated with a superscript t. Combining mechanical equilibrium and mass balance into one expression, we get

$$\begin{aligned}&\int_\Omega \left[(\boldsymbol{\sigma}:\nabla\mathbf{v})+dt(\nabla\mu)\cdot(\nabla q)+(\nabla\cdot\mathbf{u})\,q\right]dV\\&=\int_\Omega \left[(\mathbf{b}\cdot\mathbf{v})+(\nabla\cdot\mathbf{u}^t)\,q\right]dV+\int_{\partial\Omega_t}(\mathbf{t}\cdot\mathbf{v})\,dS+\int_{\partial\Omega_R}dt(\nabla\mu\cdot\mathbf{n})\,q\,dS\end{aligned} \tag{23}$$

This variational problem is solved using the general purpose PDE solver FEniCS. While the backward Euler formulation is implicit and stable, the nearly incompressible mechanical response of the gel can cause numerical convergence problems. One solution to this problem is to use mixed Taylor-Hood elements in which the interpolation function for the scalar chemical potential is taken to be one order less than that for the displacement field. The domain is

discretized by 3D hexahedral elements with quadratic interpolation for the displacement and linear interpolation for the chemical potential field.

4.6. Numerical Exploration of Typical Poroelastic Swelling and Drying Response

We now discuss the swelling and drying response of linear poroelastic materials with a view of exploring the influence of the various material parameters. Swelling/drying simulations were performed on a rectangular parallelepiped of dimensions $a\times b\times c$ which represents one-eighth symmetry model of the actual specimen. The three back planes corresponding to $x_i=0$ are provided with symmetry boundary conditions for displacements and zero flux Neumann conditions for the chemical potential. The three front planes, $x_1=10$, $x_2=10/3$, $x_3=1$ are subjected to traction free boundary conditions, and Robin boundary conditions for the chemical potential. After a convergence study, it was found that discretization of the domain into $(20\times5\times5)$ elements provided acceptable values of the strain variation. In comparing the simulation results to experimental results, the average strain over the surface is used, in keeping with the experimental procedure.

Before discussing the influence of all the material parameters, we examine how α_R of the Robin boundary influences strain evolution. Figure 4a shows the strain as a function of time with all material parameters fixed at the values indicated in the figure caption, while varying α_R. It is clear that the rate of swelling/drying increases with α_R. When $\alpha_R\to\infty$, as a Dirichlet boundary condition is approached, there is a sharp jump of strain at the starting time, which can be reduced by using a finer mesh (Bouklas et al 2015). If we rescale time by $1/\alpha_R$, the strain evolution curves collapse nearly onto one curve for early time as indicated in the inset graph in Figure 4a where time is plotted on log-scale to visualize early times more clearly; thus, we can use α_R to scale time in the following.

Simulations using this formulation permit the determination of the spatial and temporal variation of the strain and chemical potential fields during swelling and drying. Such simulations can be used to extract material parameters of linear poroelasticity through comparison to experiments. But before we embark on this, it is instructive to identify the influence of the different material parameters on the swelling and drying response. Towards this end, let us examine the equilibrium state corresponding to a gel with an initial chemical potential μ_0 equilibriating in an environment maintained at a chemical potential μ_∞. Assuming that at equilibrium the gel is stress free, the magnitude of the isotropic strain state can be obtained from Eq.(15) to be

$$\varepsilon=\frac{A(\mu_\infty-\mu_0)}{2+3\lambda} \tag{24}$$

Clearly the strain at equilibrium is proportional to the chemical potential difference, and in the linear regime, scales with the ratio of A/λ, assuming $3\lambda\gg2$. By the linear theory of

poroelasticity, the transient solution for the strain on the surface of the specimen is then expected to be of the form

$$\varepsilon(t) = \frac{A(\mu_\infty - \mu_0)}{3\lambda} f(t) \tag{25}$$

with $f(t)$ going from zero to one as t increases from zero to infinity. As noted earlier, time was normalized by $\tau_1 = l^2 / m\nu k_B T$ in Eq.(14), but the time evolution of the strain is governed by the effective diffusivity D^* or τ_2, and the parameter α_R in the Robin boundary condition in Eq.(19) and hence the time should be rescaled by the ratio $A/(\lambda\alpha_R)$.

Figure 4b shows the swelling and drying strain on the surface as a function of the normalized time. It was verified that normalizing strain by $A(\mu_\infty - \mu_0)/(3\lambda)$ and time by the ratio $A/(\lambda\alpha_R)$ resulted in the collapse of the strain vs time indicated in Eq.(25). It was found that a sum of three exponentials in time (shown in the caption to Figure 4) was adequate to fit the function $f(t)$.

4.7. The Chemical Potential and Calibration of the Material Parameters

Unlike in many of the recent experiments on gels where the gel is fully immersed in an aqueous solvent, the environment in our swelling/drying experiments is controlled by the relative humidity in an environmental chamber. In order to determine the boundary and initial conditions for swelling/drying, we need to determine the chemical potential of water both in the specimen (as prepared) and in the environmental chamber. The chemical potential for water vapor in air is defined as follows:

$$\mu - \mu_s = k_B T \log(RH) \tag{26}$$

where $\mu_s = 0$ is the saturation chemical potential, and RH is the relative humidity. At room temperature, we take $k_B T = 4\times10^{-21}$ J. Initially, we used two states for the environment in which swelling and drying are examined: RH = 100% and 15% corresponding to two chemical potentials, $\mu_{\text{swell}}/(k_B T) = 0$ and $\mu_{\text{dry}}/(k_B T) = -1.897$, respectively.

The gel, as-manufactured, contains an initial concentration of water; the rate of swelling/drying that is observed in the experiments will depend on the initial chemical potential of water in the gel in comparison to the chemical potential of water in the environment. We considered three different environments in order to determine the initial chemical potential. When the gel specimens of composition A or B are (i) fully immersed in pure water, (ii) fully immersed in water/glycerol mixture of the same ratio as in compositions A or B, and (iii) placed in a chamber with controlled humidity. In condition 1, the water diffuses into the gel while the glycerol diffuses out of the gel and dissolves into the environment; since this changes the composition continuously, this case is not considered further in the present work. In condition 2, due to the mobility of both the water and glycerol, the gelatin network might expand but preferential migration of glycerol and/or water might occur and therefore this is also not

considered here. Condition 3 is the most appropriate since in this case, water may diffuse in or out of the gel depending on the RH of the environment, but there is no driving force for migration of glycerol.

Let us denote the chemical potential of water in the as-manufactured gel of the two different compositions as μ_A and μ_B respectively; we use two methods to determine these values. First, we use the experimentally measured initial swelling and drying rates, $\dot{\varepsilon}_{\text{swell}}$ and $\dot{\varepsilon}_{\text{dry}}$ respectively, to determine the initial chemical potential in the gel. In the linear poroelastic regime, the initial swelling and drying rates are expected to be proportional to the chemical potential difference and hence,

$$\frac{\dot{\varepsilon}_{\text{swell}}}{\dot{\varepsilon}_{\text{dry}}} = \frac{\mu_{\text{swell}} - \mu_A}{\mu_{\text{dry}} - \mu_A} \tag{27}$$

A similar expression holds for composition B. Based on the measured rates from the early time data in Figure 3, we determined the initial chemical potential in the two compositions as: $\mu_A = -0.3124$ and $\mu_B = -0.1638$. These values of the chemical potential were confirmed by a second method, in which the gels of composition A and B were kept at RH (73% and 85%) corresponding to the estimated μ_A and μ_B so that they were at chemical equilibrium and showed no swelling or drying; these results are also shown in Figure 3 by the gray and black lines.

Next, we turn attention to the determination of the poroelastic parameters. According to Sections 4.3 and 4.4, there are five parameters $\left(\lambda^{\text{dr}}, G, \nu, D^*, \alpha_R\right)$ that need to be determined. We denote $\varepsilon_e(t)$ and $\varepsilon_s(t)$, respectively, as the strains from the experiment and the corresponding simulation. Based on the discussion in Session 4.6 about the scaling of the strain, we can write:

$$\varepsilon_s\left(\bar{t}; \frac{A}{\lambda}\right) = \frac{A\left(\mu_\infty - \mu_0\right)}{3\lambda} f\left(\bar{t}\right) \tag{28}$$

We note that the real time t and the scaled time $\bar{t}$ are related through: $\bar{t} = \dfrac{\alpha_R t}{\tau_2}$; for water as the solvent, we take $\nu = 3\times10^{-29}\ \text{m}^3$. Therefore, we seek two parameters $\left(\tau_2/\alpha_R, A/\lambda\right)$ by minimizing the difference between the simulated strain evolution and the measured strain:

$$e = \left\| \frac{\varepsilon_e(t)}{\mu_\infty - \mu_0} - \frac{A}{3\lambda} f\left(\frac{\alpha_R t}{\tau_2}\right) \right\| \tag{29}$$

The experimental data is shown in Figure 5 with the strain rescaled by $\left(\mu_\infty - \mu_0\right)$ and it is seen to collapse into a single curve as predicted by the linear theory for about the first 2.5 hours. The minimization process is equivalent to fitting the measured data $\varepsilon_e(t)/\left(\mu_\infty - \mu_0\right)$ for first 2.5

hours to a function $af\left(t/b\right)$, where $a=A/\left(3\lambda\right)$ and $b=l^2/\left(\alpha_R D^*\right)=\tau_2/\alpha_R$. The best fit curve is shown in Figure 5 and is seen to be a good representation of the experimental data for the first 2.5 hours. From the fitting process, we obtain $a=0.8558$ and $b=58.92$ hours. Using a modulus $G=33$ kPa obtained from a uniaxial tensile test, and setting $D^*=1.6\times10^{-11}$ m^2/s from Baumberger (2003), we obtain $A\sim4000$, $\lambda=1558$, and $\alpha_R\sim0.66$ with the length scale $l=0.0015m$. It should be noted, however, that beyond about 2.5 hours, there is a marked departure between the measured and calculated responses both for swelling and for drying. It appears that a fully nonlinear poroelastic modeling is necessary for adequately representing the material behavior beyond the early stage; such models have been presented over the past decade (see Hong et al. 2008, 2009; Chester and Anand, 2010; Bouklas and Huang, 2012; Bouklas et al. 2015 and others). We will explore this in the next section.

5. Nonlinear poroelasticity

We now describe the nonlinear poroelastic theory that will be used to interpret the swelling/drying data obtained in Section 3 beyond the linear regime. The model description follows the work of Hong et al (2008, 2009), Chester and Anand, (2010), Bouklas and Huang, (2012) and Bouklas et al (2015). Standard nonlinear continuum mechanics notation is used. Briefly, the problem is formulated in the reference configuration which is taken to be the dry network condition; material points which occupy the position $\mathbf{X}$ in the reference state are deformed to $\mathbf{x}\left(\mathbf{X}\right)$ due to swelling, drying, or mechanical loading. The deformation gradient tensor is defined as $\mathbf{F}=\nabla\mathbf{x}\left(\mathbf{X}\right)$, or in component form $F_{iK}=\partial x_i/\partial X_K$, with $\left(i,K\right)$ taking the range $\left(1,2,3\right)$. In the Flory-Rehner nonlinear theory, the free energy of the system is taken to be a function of both the concentration of the solvent in the gel and the deformation gradient tensor as discussed below.

5.1. Flory-Rehner Nonlinear Constitutive Models

The free-energy function is taken to be the Flory-Rehner model for the gel. This is written as

$$\frac{\hat{U}\left(\mathbf{F},C\right)}{Nk_BT}=\frac{1}{2}\left[I_c-3-2\ln\left(J\right)\right]-\frac{1}{N\nu}\left[\nu C\ln\left(\frac{1+\nu C}{\nu C}\right)+\frac{\chi}{1+\nu C}\right] \tag{30}$$

Here, the free energy normalized by Nk_BT, is written as a function of $\mathbf{F}$, the deformation gradient tensor and C, the nominal concentration of the solvent in the gel. In addition, N is the number of polymer chains per unit reference volume, ν is the volume of the solvent molecule, k_B is the Boltzmann constant, T is the temperature, $I_c=F_{iK}F_{iK}$, and $J=\det\left(\mathbf{F}\right)$, the determinant of the deformation gradient tensor. The first term on the right hand side corresponds to the stretching response of the network. The second term arises from the entropy and enthalpy

of mixing, with $\chi \sim 0-1.2$. At equilibrium, one can define the nominal stress and chemical potential as follows:

$$s_{iJ} = \frac{\partial \hat{U}(\mathbf{F},C)}{\partial F_{iJ}},\ \mu = \frac{\partial \hat{U}(\mathbf{F},C)}{\partial C} \tag{31}$$

Alternatively, the deformation gradient and chemical potential may be taken as the independent variables, once the volume change in the gel is attributed entirely to changes in concentration of the solvent. If we take $1+\nu C = J$ to insist that any volume change is only due to change in the solvent concentration, and define $U(\boldsymbol{F},\mu) = \hat{U}(\boldsymbol{F},C) - \mu C$, the free-energy may be re-written in terms of the deformation gradient and the chemical potential:

$$\frac{U(\mathbf{F},\mu)}{Nk_BT} = \frac{1}{2}\left[I_c - 3 - 2\ln(J)\right] - \frac{1}{N\nu}\left[(J-1)\ln\left(\frac{J}{J-1}\right) + \frac{\chi}{J}\right] - \frac{\mu/(k_BT)}{N\nu}(J-1) \tag{32}$$

The normalized free energy function depends on $\mathbf{F}$ and μ/k_BT and contains only two dimensionless material constants: $N\nu \sim 10^{-4}-10^{-1}$ and $\chi \sim 0-1.2$.

The nominal stress is then obtained as

$$\frac{s_{iJ}}{Nk_BT} = \left[F_{iJ} - H_{iJ}\right] + \frac{1}{N\nu}\left[J\ln\left(\frac{J-1}{J}\right) + 1 + \frac{\chi}{J} - \frac{\mu}{k_BT}J\right]H_{iJ} \tag{33}$$

where $H_{iJ} = \frac{1}{J}\frac{\partial J}{\partial F_{iJ}}$. The gel is typically formed from a heated mixture of the solvent and polymer chains as the mixture cools below the gelation temperature. Hence, at the gelated state, the gel is isotropically swollen by λ_0 relative to the dry state, and contains a certain concentration of solvent, C_0 or equivalently is at equilibrium with a chemical potential, μ_0. And, at this state we have $s_{iJ} = 0$; hence setting the nominal stress to zero in Eq.(33), we obtain the relationship between the initial stretch and chemical potential:

$$\frac{\mu_0}{k_BT} = N\nu\left[\frac{1}{\lambda_0} - \frac{1}{\lambda_0^3}\right] + \ln\left(1 - \frac{1}{\lambda_0^3}\right) + \frac{1}{\lambda_0^3} + \frac{\chi}{\lambda_0^6} \tag{34}$$

Hence, the gels of composition A and B are at initial stretches λ_0^A and λ_0^B, respectively. We note that the stress and chemical potential are already in a non-dimensional form.

5.2. Mechanical Equilibrium

Swelling and drying are time-dependent processes, governed by diffusion of the solvent molecules through the gel. This diffusive process is rather slow in comparison to stress-wave propagation within the gel so that mechanical equilibrium equations could be imposed on the gel. It is not readily apparent, however, whether the viscoelastic processes could be neglected.

Hence, mechanical equilibrium requires that

$$\begin{aligned} &s_{iJ,J} + f_i = 0 \quad for \quad \mathbf{X} \in \Omega \\ &s_{iJ} N_J = T_i \quad for \quad \mathbf{X} \in \partial\Omega_t \end{aligned} \tag{35}$$

where f_i are the nominal body force components (per unit reference volume), Ω is the volume in the reference configuration, $\partial\Omega_t$ is the surface (with unit normal $\mathbf{N}$) over which nominal tractions are prescribed to be T_i. Note that displacement boundary conditions may be prescribed on the complementary boundary $\partial\Omega_u$.

5.3. Fluid flux

The fluid flow is commonly modeled using Darcy's law in linear poroelasticity. Hong et al (2008) provided a detailed discussion of the calculations for a finitely deforming gel. The essential ingredient is in adopting a diffusion model for the true flux in the deformed configuration and rewriting it in terms of nominal quantities in the reference configuration. The starting point is the assumption that the true flux, j_k, is proportional to the gradient of the chemical potential in the current state:

$$j_k = -\frac{cD}{k_B T}\frac{\partial \mu}{\partial x_k} \tag{36}$$

Here, c is the concentration in the current configuration, and related to the nominal concentration by $C = cJ$; D is the solvent diffusivity, assumed to be a constant. The true flux and nominal flux are related by $j_k n_k dS = J_K N_K dS_0$, where the differential areas in the current and reference configurations are related by Nansen's formula: $F_{iK} n_i dS = J N_K dS_0$. The nominal flux can then be calculated to be

$$J_K = -\frac{CD}{k_B T}\left(\frac{\partial X_K}{\partial x_k}\frac{\partial X_L}{\partial x_k}\right)\frac{\partial \mu}{\partial X_L} \tag{37}$$

The term multiplying the gradient of the chemical potential is defined as the mobility tensor, $\mathbf{M}$:

$$M_{KL} = \frac{CD}{k_B T}\left(\frac{\partial X_K}{\partial x_k}\frac{\partial X_L}{\partial x_k}\right) \tag{38}$$

Mass conservation then provides the governing equation for solvent diffusion:

$$\begin{aligned} &\frac{\partial C}{\partial t} + \frac{\partial J_K}{\partial X_K} = 0 \quad for \quad \mathbf{X} \in \Omega \\ &J_K N_K = -g \quad for \quad \mathbf{X} \in \partial\Omega_f \end{aligned} \tag{39}$$

where $\partial\Omega_f$ is the surface (with unit normal $\mathbf{N}$) over which normal flux of the solvent *into* the solid is prescribed to be g. Similar to the displacement boundary conditions for the mechanical problem, chemical potential may be prescribed on the complementary boundary $\partial\Omega_\mu$. Note that a Robin boundary condition, similar to that discussed for the linear problem could also be used.

5.4. Normalized Form

As indicated in Section 5.1, free energy and chemical potential are normalized as:

$$\bar{U} = \frac{U(\mathbf{F},\mu)}{Nk_BT},\ \bar{\mu} = \frac{\mu}{k_BT} \tag{40}$$

and concentration, time, and length are scaled as:

$$\bar{C} = C\nu,\ \bar{t} = \frac{Dt}{l^2} \text{ and } \bar{\mathbf{X}}_K = \frac{\mathbf{X}_K}{l} \tag{41}$$

Normalizing the flux as $\bar{J}_K = \frac{\nu l}{D} J_K = -(J-1)\left(\frac{\partial \bar{X}_K}{\partial \bar{x}_k}\frac{\partial \bar{X}_L}{\partial \bar{x}_k}\right)\frac{\partial \bar{\mu}}{\partial \bar{X}_L}$, the conservation equation in non-dimensional form may be written as:

$$\frac{\partial J}{\partial t} + \frac{\partial J_K}{\partial X_K} = 0 \tag{42}$$

where the bars have been removed from all normalized quantities in Eq.(42) and thereafter.

As discussed in Section 4.4, neither the Dirichlet nor the Neumann boundary condition will be used for the boundaries exposed to the environment of controlled humidity in the present study. Instead, we use the Robin condition, now expressed in the current (deformed) configuration as:

$$j_k n_k = \alpha_r(\mu - \mu_\infty) \tag{43}$$

where α_r is a constant. In order to relate this to the linear theory, which was calibrated in the vicinity of the initial state with an initial stretch λ_0, the flux is approximately:

$$j_k = -\frac{C_0}{J_0}\frac{\partial \mu}{\partial x_k} = -\frac{J_0 - 1}{J_0}\frac{\partial \mu}{\partial x_k} \tag{44}$$

Substituting for the chemical potential gradient from the Robin boundary used in the linear theory, we obtain

$$j_k n_k = -\frac{J_0 - 1}{J_0}\frac{\partial \mu}{\partial x_k} n_k = \frac{J_0 - 1}{J_0}\alpha_R(\mu - \mu_\infty) \tag{45}$$

Comparing Eqs.(43) and (45), we get

$$\alpha_r = \frac{J_0 - 1}{J_0}\alpha_R \tag{46}$$

The true flux and nominal flux are related by $j_k n_k dS = J_K N_K dS_0$; substituting this into Eq.(45), and using the fact that $\lambda_N dS = J dS_0$, where $\lambda_N = \sqrt{\mathbf{F}^T \mathbf{F}\mathbf{N}\cdot\mathbf{N}}$ is the stretch perpendicular to the surface, we get the normal component of the nominal flux:

$$J_K N_K = j_k n_k \frac{J}{\lambda_N} = \frac{(J_0 - 1)J}{\lambda_N J_0}\alpha_R(\mu - \mu_\infty) \tag{47}$$

which can be used in the weak form described in the next section.

5.5. The Weak Form

The weak-form of the governing equations are obtained by considering test functions $\mathbf{v}$ and q for the displacement vector field and chemical potential scalar field, respectively.

Similarly, the mass balance equation yields

$$\int_\Omega \left[\frac{\partial J}{\partial t} q - J_K q_{,K}\right] dV = -\int_{\partial\Omega_g} J_K N_K q dS \tag{48}$$

Using a backward Euler scheme for the time derivative term in the above, an incremental formulation is written as

$$\int_\Omega \left[\left(J - J^t\right) q - \Delta t J_K q_{,K}\right] dV = \Delta t \int_{\partial\Omega_g} J_K N_K q dS \tag{49}$$

The weak form for the displacement vector field is equivalent to potential energy minimization; when the stored strain energy is provided explicitly, an alternative formulation may be adopted without calculation of the stress. Consider the total potential energy:

$$\Pi = \Pi_{\text{int}} + \Pi_{\text{ext}} = \int_\Omega U\left(\mathbf{F}(\mathbf{u}), \mu\right) dV + \int_\Omega \left[\mathbf{b}\cdot\mathbf{u}\right] dV + \int_{\partial\Omega_t} \left[\mathbf{T}\cdot\mathbf{u}\right] dS \tag{50}$$

The solution displacement vector field should minimize the total potential energy above, which means that the directional derivative of energy will be zero for all possible variations of $\mathbf{u}$: thus,

$$P(\mathbf{u}, \mathbf{v}, \mu) = \left.\frac{\partial \Pi(\mathbf{u} + \varepsilon\mathbf{v}, \mu)}{\partial \varepsilon}\right|_{\varepsilon = 0} = 0 \tag{51}$$

Combining potential energy minimization and mass balance into one expression, we get

$$\int_\Omega \left[\left(J - J^t\right) q - \Delta t J_K q_{,K}\right] dV + P(\mathbf{u}, \mathbf{v}, \mu) - \Delta t \int_{\partial\Omega_g} J_K N_K q dS = 0 \tag{52}$$

This form can be implemented directly in FEniCS, and is used in the following. Once again, mixed Taylor-Hood elements in which the interpolation function for the scalar chemical potential is taken to be one order less than that for the displacement field will be used.

5.6. Verification of the Finite Element Simulation

To verify the accuracy of the FEniCS formulation of the nonlinear model, we compare the simulation results for the problem of swelling of a constrained hydrogel layer to the analytic and numerical results in Bouklas et al (2015). We consider an infinite hydrogel layer of thickness h_0, with the bottom surface attached to a rigid, impermeable substrate and the top surface exposed to the solvent at fixed chemical potential. We note that Bouklas et al (2015) considered a nearly incompressible hydrogel in their numerical simulation, but they show little difference from the analytical incompressible limit.

We consider a rectangular parallelopiped of dimension $\left(l_0 \times w_0 \times h_0\right)/\lambda_0$ swollen isotropically to a chemical potential μ_0 and initial stretch λ_0, resulting in the initial gel of dimension $\left(l_0 \times w_0 \times h_0\right)$, see Figure 6. The gel is then subject to constrained swelling boundary conditions. We implement a 3D model in FEniCS with the following boundary conditions imposed, see Figure 7. The top surface $\left(S_1, x_3 = 1\right)$ is traction free and its chemical potential is fixed at 0; the bottom surface $\left(S_2, x_3 = 0\right)$ is at fixed displacement $\left(\mathbf{u} = \tilde{\mathbf{u}}_0\right)$ and its flux is zero; the left and right surfaces $\left(S_3, x_2 = 0,1\right)$ are subject to symmetry condition with $u_2 = u_{20}$, $T_{21} = T_{23} = 0$ and $J_2 = 0$; the front and back surface $\left(S_4, x_1 = 0,1\right)$ are also subject to symmetry condition $u_1 = u_{10}$, $T_{12} = T_{13} = 0$ and $J_1 = 0$. The initial chemical potential is taken to be μ_0, and the corresponding initial stretch λ_0 can be calculated from Eqn. (31); the initial displacement is then $\tilde{\mathbf{u}}_0 = \left\{u_{x0}, u_{y0}, u_{z0}\right\} = \left(\lambda_0 - 1\right)\mathbf{X}$. The following parameters were used in the simulations: $\lambda_0 = 1.4$, $\chi = 0.4$, and $N\nu = 0.001$. We use twenty elements along thickness as used in Bouklas et al (2015). We noted that Bouklas et al used a 2D-FE model in their simulations, but the result should be comparable to the 3D simulations. The self-similar solution, obtained from the linearized diffusion equation, predicts that the thickness changes at early time should be proportional to square root of time (Bouklas and Huang, 2012). The change of thickness with time, calculated with the 3D model is compared with the numerical results and the self-similar solution of Bouklas et al (2015) in Figure 8. The 3D result (red solid line) and the 2D result (black dash line) are nearly on top of each other; and both simulations exhibit a small difference from the analytical self-similar solution (blue solid line) for the early time, probably caused by the coarse mesh, as discussed by Bouklas et al (2015). We take this as verification of FE formation in FEniCS.

5.7. *Simulation of Free Swelling and Comparison to Experimental Data*

For the nonlinear theory, there are five parameters that need to be determined: $\left(N, \chi, D, \alpha_R\right)$ and the initial swelling ratio, λ_0. We will determine the three parameters $\left(N, \chi, \lambda_0\right)$ in the following.

First, the initial swollen stretch λ_0 and the chemical potential μ_0 are related by Eqn. (34). Second, from the experimental data, though the swelling process was still in progress, the drying process reached equilibrium stage at about 100 hours; therefore, the final drying stretch, $\lambda_d = (1+\varepsilon_d)\lambda_0$, where ε_d is determined from strain measurement, is related to the drying chemical potential μ_{dry} as:

$$\mu_{\text{dry}} = N\nu\left[\frac{1}{\lambda_d} - \frac{1}{\lambda_d^3}\right] + \ln\left(1 - \frac{1}{\lambda_d^3}\right) + \frac{1}{\lambda_d^3} + \frac{\chi}{\lambda_d^6} \tag{53}$$

Finally, the normalized shear modulus is related to the initial stretch as

$$G = \frac{1}{\lambda_0} = \frac{33\ \text{kPa}}{Nk_BT} = \frac{2.475\times10^{-4}}{N\nu} \tag{54}$$

where the dimensional shear modulus is taken to be 33 kPa based on a uniaxial tension test. Hence, for each gel composition, we can determine the three parameters (N, χ, λ_0), by solving the three equations (34), (53) and (54). As indicated in Section 4, we have determined $\mu_0 = -0.3124$, $\mu_{\text{dry}} = -1.897$ and $\varepsilon_d = -0.14$ for specimen with composition A, and $\mu_0 = -0.1638$, $\mu_{\text{dry}} = -1.897$ and $\varepsilon_d = -0.18$ for specimen with composition B. Then, from Eqs. (34, 53 and 54) we obtain: $N \sim 10^{25}$, $\chi \sim 0.007$, and $\lambda_0 \sim 1.186$ for composition A and, $N \sim 10^{25}$, $\chi \sim 0.2007$, and $\lambda_0 \sim 1.240$ for composition B.

For the determination of the diffusivity and α_R, we compare the free swelling/drying experiments to numerical simulations of the same problem with the nonlinear finite element method. The Taylor-Hood hexahedral elements are used with quadratic interpolation for the displacement vector field and linear interpolation for the chemical potential field. Since the gradient of chemical potential is much larger in the thickness direction, a coarse mesh will cause large oscillation near boundary with small time steps; this was explored as shown in Figure 9. Figure 9a shows the chemical potential variation across the thickness for different mesh sizes while Figure 9b shows the chemical potential at the point (0,1,0) as a function of time. This convergence study indicated that the 3D domain discretized by a $(6 \times 3 \times 40)$ mesh was adequate. Adaptive time stepping was used with an initial time step of 0.00005 normalized time units, decreasing by a half when the solver failed to converge after eight iterations and doubling when the solver converges within five iterations. The largest time step was constraint to not exceed 0.2 in order to maintain accuracy of the solution.

In order to determine α_R for both compositions, simulations of different set parameters are calculated for both composition A and B for drying case. Figure 10a shows that α_R will influence the shape of the strain versus real time curves. Through a parameter sweep process, we found that $\alpha_R = 1.5$ was the most suitable for fitting the experimental curves for both

compositions. The comparison of strain versus time curves between the experimental results and the nonlinear simulations using α_R obtained is shown in Figure 10b. The nonlinear simulations predict nearly same strain evolution as experiments and capture the asymmetry between the swelling and drying process. There is a small disagreement between the simulations and experiments that arises at the later stages of swelling test; this may be due to departure from the neo-Hookean model at larger stretch levels and needs to be explored further. The diffusion coefficient D was estimated by assessing a time constant of about 7.6 hours for composition A and 8.4 hours for composition B; this yields an estimate of the diffusion coefficient: $D = 8.2 \times 10^{-11} m^2/s$ for composition A and $D = 7.4 \times 10^{-11} m^2/s$ for composition B.

5.8. *Linear and nonlinear parameters comparison and summary*

Parameters of linear and nonlinear theory extracted as indicated above are listed in Table 2. We can compare these calibrations by linearizing the nonlinear theory; the parameters are related by (Bouklas and Huang, 2012):

$$G = \frac{Nk_B T}{\lambda_0} \tag{55}$$

$$\lambda^{\mathrm{dr}} = G\frac{1-\kappa}{\kappa};\ \kappa = N\nu\left[\frac{1}{\lambda_0^2\left(\lambda_0^3-1\right)} + \frac{N\nu}{\lambda_0^2} - \frac{2\nu}{\lambda_0^3}\right]^{-1} \tag{56}$$

$$D^* = DN\nu\left(2 + \frac{\lambda^{\mathrm{dr}}}{G}\right)\frac{\lambda_0^3 - 1}{\lambda_0^4} \tag{57}$$

We calculate the parameters of the linear poroelasticity from the nonlinear theory, listed in Table 3, which are comparable to the value we determined from the linear simulation. From the parameters determination procedure, we conclude that: i) the shear modulus needs to be determined elsewhere, such as from a tension test. ii) α_R from the Robin boundary condition and the diffusivity D or effective diffusivity D^* both influence diffusion time, and could not be determined separately for the linear theory. But in the nonlinear theory, since α_R also influences the shape of the drying curve, both α_R and D can be estimated by fitting to the drying data. Thus all parameters of the nonlinear theory except for the shear modulus can be determined from the swelling/drying experiments.

6. Summary

The main goal of this work is to explore the poroelastic swelling and drying behavior of gelatin-glycerol-water hydrogel experimentally, and to interpret the results in the framework of linear and nonlinear poroelastic theories. Towards this end gelatin gels were prepared by mixing pig-skin derived collagen in different mixtures of glycerol and water. The resulting gels exhibited significant poroelastic swelling and drying when exposed to environmental conditions of 100% RH and 15% RH, respectively. A significant time asymmetry in the swelling/drying responses was observed.

A linear poroelastic model was formulated for finite element simulations using FEniCS. Special attention was paid to the boundary condition between the gel and the environment; in particular, the use of a Robin boundary condition relating the flux to the difference in the chemical potential was found to be important. While the linear poroelastic model was found to be suitable for capturing swelling and drying for the first few hours, it was not suitable for determining the long time behavior, suggesting the need for a nonlinear theory accounting for large stretches that occur at longer times. In particular, the time asymmetry between the swelling and drying responses could not be captured by the linear poroelastic formulation.

The shortcomings of the linear theory are addressed with a nonlinear theory based on Flory-Rehner model. This model was also formulated for numerical solutions with the software FEniCS to simulate free swelling and drying processes. The nonlinear theory was found not only to capture the time asymmetry behavior between drying and swelling, but also to reproduce the long-term strain versus time evolution observed in the experiments, thereby permitting calibration of the material parameters of the gel through swelling/drying experiments. However, deviations from the nonlinear theory was still observed at large swelling strains; this may require the use of a non neo-Hookean constitutive model, such as the Gent model; this will be explored in future work.

Acknowledgements

This work was performed during the course of an investigation into the behavior of hydrogels funded by the National Science Foundation through a grant CMMI-1538658. This support is gratefully acknowledged.

Declaration of interests

☒ The authors declare that they have no known competing financial interests or personal relationships that could have appeared to influence the work reported in this paper.

☐The authors declare the following financial interests/personal relationships which may be considered as potential competing interests:

References

Alnaes MS, Blechta J, Hake J, Johansson A, Kehlet B, Logg A, Richardson C, Ring J, Rognes ME, Wells GN, 2015, The FEniCS Project Version 1.5, *Archive of Numerical Software*, **3**.

Anand L, 2015. Drucker Medal Paper: A derivation of the theory of linear poroelasticity from chemoelasticity, *Journal of Applied Mechanics*, **82**, 111005.

Baumberger T, Caroli C, Martina D, 2006, Solvent control of crack dynamics in a reversible hydrogel, *Nature Materials*, **5**, 552-556.

Biot M, 1941, General theory of three-dimensional consolidation, *Journal of Applied Physics*, **12**, 155-164.

Bouklas N and Huang R, 2012, Swelling kinetics of polymer gels: comparison of linear and nonlinear theories, *Soft Matter*, **8**, 8194-8203.

Bouklas N, Landis CM, Huang R, 2015. A nonlinear, transient finite element method for coupled solvent diffusion and large deformation of hydrogels, *Journal of the Mechanics and Physics of Solids*, **79**, 21-43.

Cai S, Hu Y, Zhao X, Suo Z, 2010, Poroelasticity of a covalently crosslinked alginated hydrogel under compression, *Journal of Applied physics*, **108**, 113514

Chan EP, Hu Y, Johnson PM, Suo Z, Stafford CM, 2012, Spherical indentation testing of poroelastic relaxations in thin hydrogel layers, *Soft matter*, **8**, 1492-1498

Chester SA, Anand L, 2010, A coupled theory of fluid permeation and large deformations for elastomeric materials, *Journal of the Mechanics and Physics of Solids*, **58**, 1879-1906.

De Gennes, PG, 2002, Solvent evaporation of spin case films: "crust" effects, *The European Physical Journal E*, **7**, 31-34.

Flory PJ, 1942, Thermodynamics of high polymer solution, *The Journal of Chemical Physics*, **10**, 51-61

Gibbs J, 1878, On the equilibrium of heterogeneous substances, *Transactions of the Connecticut Academy of Arts and Sciences*, Vol III, New Haven CT, 108-248.

Harrington WF and Rao NV, 1970, Collagen structure in solution. I. Kinetics of helix regeneration in single-chain gelatins, *Biochemistry*, **9**, 3714-3724.

Hong W, Liu Z, Suo Z, 2009, Inhomogeneous swelling of a gel in equilibrium with a solvent and mechanical load, *International Journal of Solids and Structures*, **46**, 3282-3289.

Hong W, Zhao X, Zhou J Suo Z, 2008, A theory of coupled diffusion and large deformation in polymeric gels, *Journal of the Mechanics and Physics of Solids*, **56**, 1779-1793.

Huggins ML, 1941, Solutions of long chain compounds, *The Journal of Chemical Physics*, **9**, 440

Lee KY and Mooney DJ, 2001, Hydrogels for tissue engineering, *Chemical Reviews*, **101**, 1869-1879.

te Nijenhuis K, 1997, Thermoreversible Networks: Viscoelastic Properties and Structure of Gels, Advances in Polymer Science, 130, Springer

Rault I, Frei V, Herbage D, Abdul-Malek A, Huc A, 1996, Evaluation of different chemical methods for cross-linking collagen gel, films and sponges, *Journal of Materials Science: Materials in Medicine*, **7**, 215-221.

Sanwlani S, Kumar P, Bohidar HB, 2011, Hydration of gelatin molecules in glyceron-water solvent and phase diagram of gelatin organogels. *Journal of Physical Chemistry B*, **115**, 7332-7340.

Tice LF, Moore AW, 1950, Solutions of gelatin in polyhydric alcohols, *Journal of the American Pharmaceutical Association*, **11**, 565-567.

Ullah F, Othman MBH, Javed F, Ahmad Z, Akil HM, 2015, Classification, processing and application of hydrogels: A review, *Materials Science and Engineering C*, **57**, 414-433

Yoon J, Cai S, Suo Z, Hayward RC, 2010, Poroelastic swelling kinetics of thin hydrogel layers: comparison of theory and experiment, *Soft matter*, **6**, 6004-6012

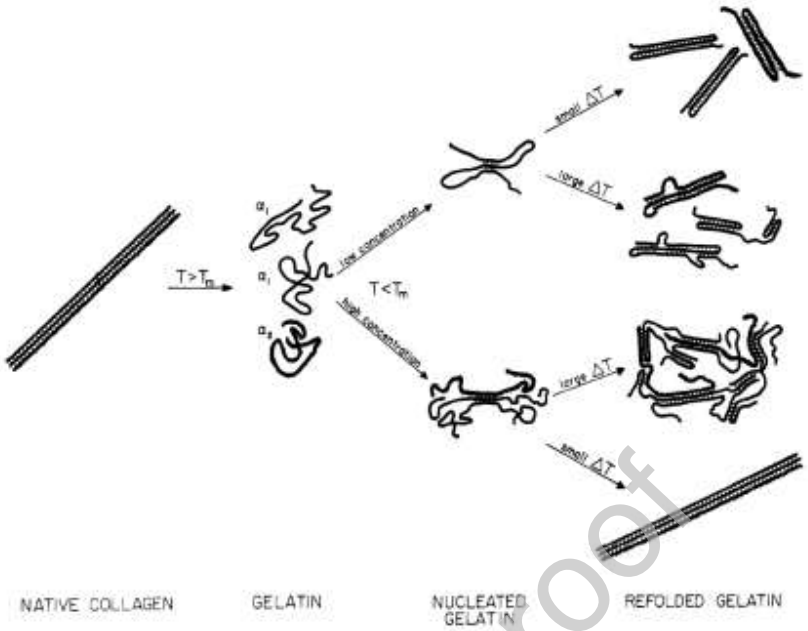

Figure 1. Formation of an entangled helical network in a gelatin gel (Reproduced with permission, Harrington and Rao, 1970)

(a) (b)

Figure 2. (a) Geometry of specimens for the drying/swelling experiments; (b) Speckle pattern used for measurement of strain using digital image correlation.

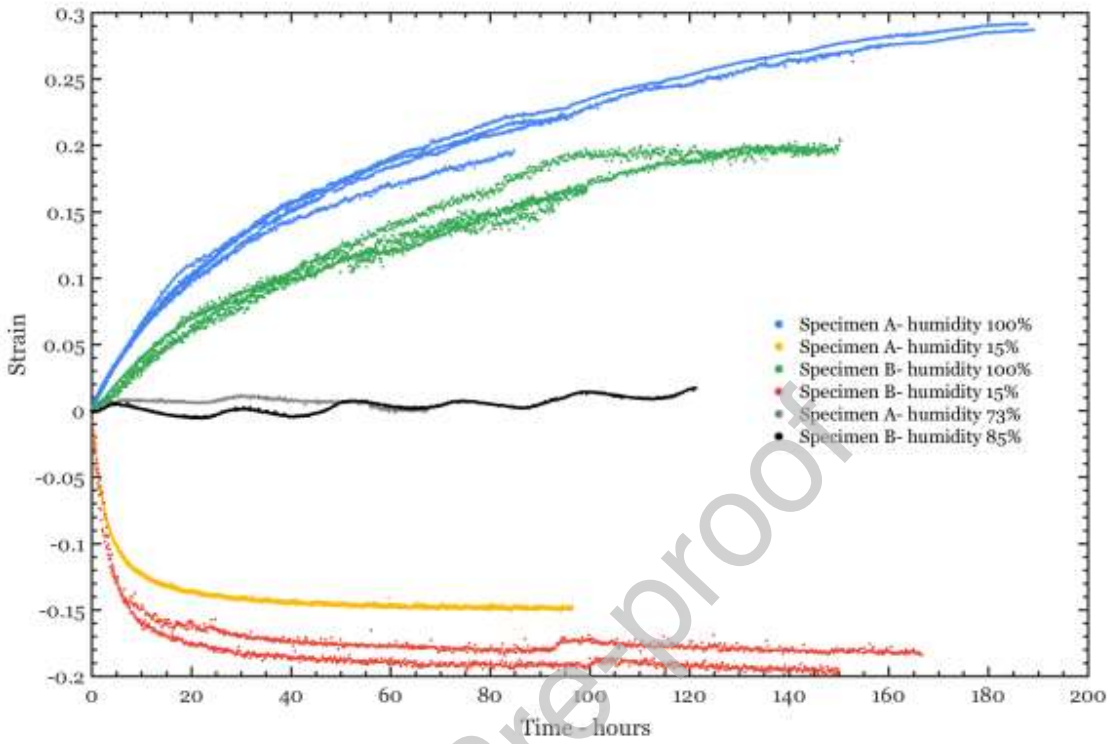

Figure 3. Time evolution of the strain in the vertical direction for swelling to 100% RH and drying to 15% RH of two different compositions of the gelatin-glycerol-water based gel. The grey and black lines correspond to environmental chemical potential equal to composition A (humidity 73%) and B (humidity 85%) respectively.

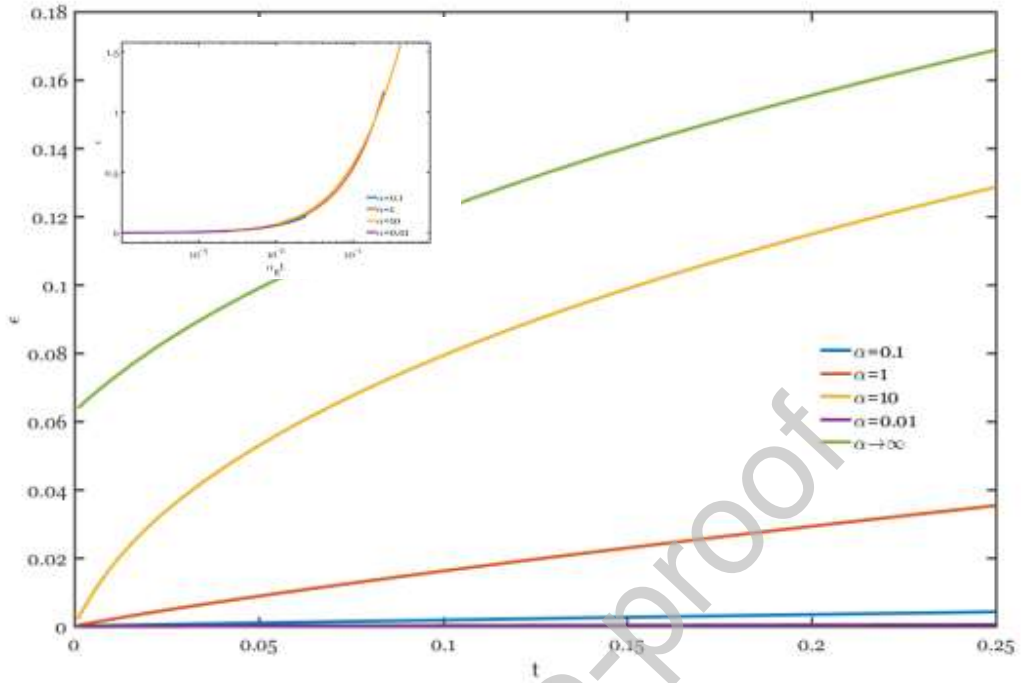
0.18
0.16
0.14
0.12
0.1
0.08
0.06
0.04
0.02
0
ϵ
0
0.05
0.1
0.15
0.2
0.25
t
α=0.1
α=1
α=10
α=0.01
α→∞

(a)

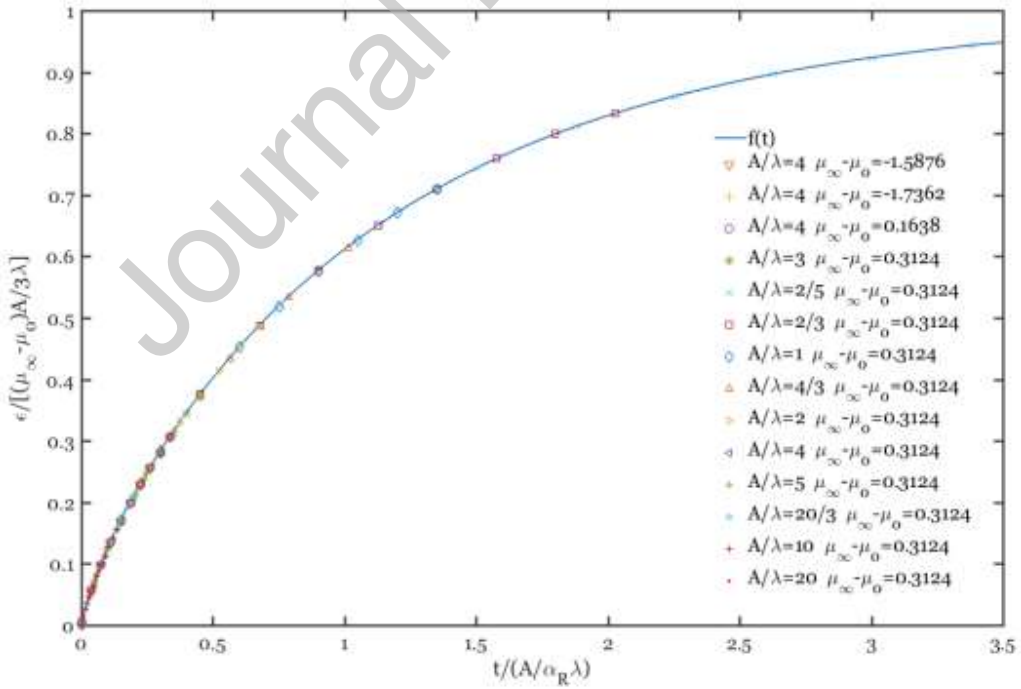
1
0.9
0.8
0.7
0.6
0.5
0.4
0.3
0.2
0.1
0
ϵ/[(μ∞-μ0)A/3λ]
0
0.5
1
1.5
2
2.5
3
3.5
t/(A/αRλ)
f(t)
A/λ=4 μ∞-μ0=-1.5876
A/λ=4 μ∞-μ0=-1.7362
A/λ=4 μ∞-μ0=0.1638
A/λ=3 μ∞-μ0=0.3124
A/λ=2/5 μ∞-μ0=0.3124
A/λ=2/3 μ∞-μ0=0.3124
A/λ=1 μ∞-μ0=0.3124
A/λ=4/3 μ∞-μ0=0.3124
A/λ=2 μ∞-μ0=0.3124
A/λ=4 μ∞-μ0=0.3124
A/λ=5 μ∞-μ0=0.3124
A/λ=20/3 μ∞-μ0=0.3124
A/λ=10 μ∞-μ0=0.3124
A/λ=20 μ∞-μ0=0.3124

(b)

Figure 4. (a) Influence of α_R on the time evolution of the swelling strain with $\mu_0 = -0.3124$, $A = 3200$, $\lambda = 2000$; the inset shows the result of rescaling by α_R. (b) Evolution of normalized swelling/drying strain $A(\mu_\infty - \mu_0)/(3\lambda)$ with normalized time $t/\left[A/(\lambda\alpha_R)\right]$; note that t is already normalized as in Eq.(14). A curve fit to the time variation based on the sum of three exponentials appears to be adequate: $f(t) = 1 - 0.0519e^{-14.41t} - 0.1179e^{-2.17t} - 0.8302e^{-0.7948t}$.

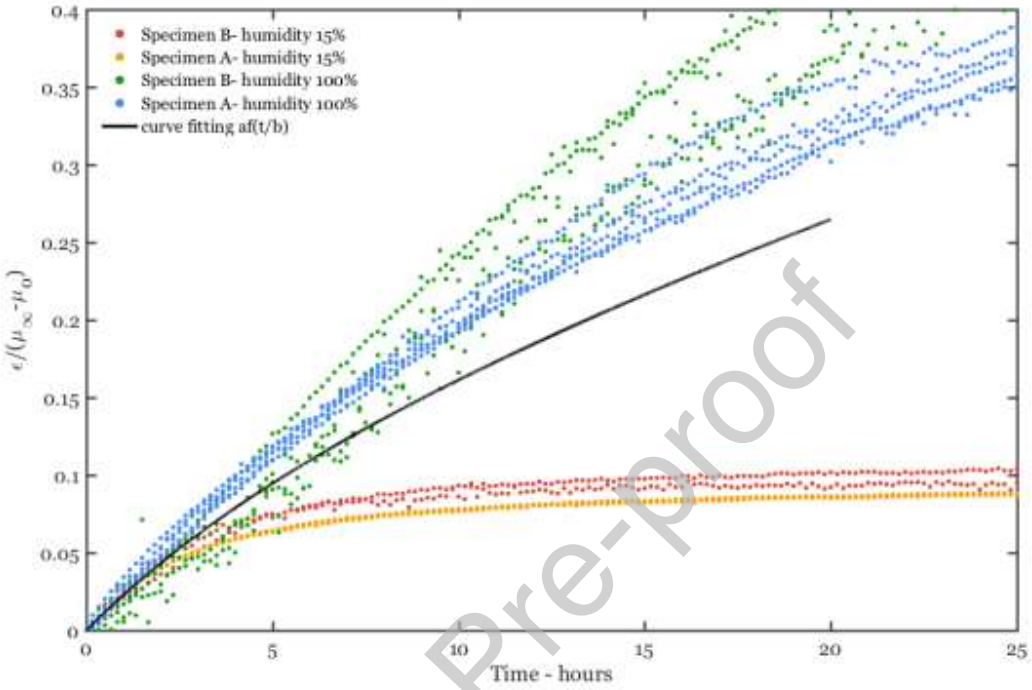

Figure 5. Comparison of the linear poroelastic calculation to the experiments reported in Figure 3.

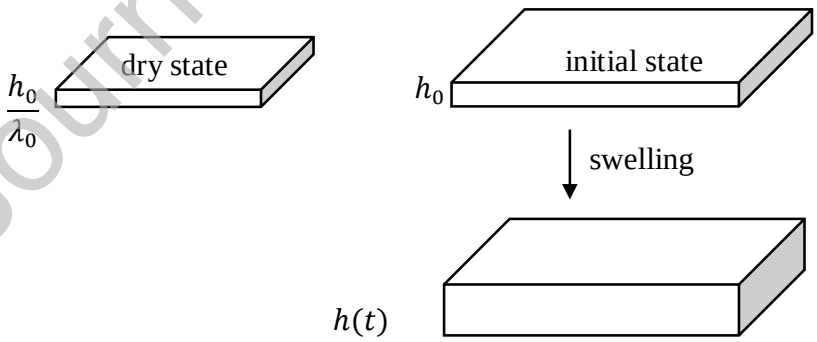

Figure 6 Schematic illustration of swelling of a finite hydrogel layer of thickness h_0 with isotropic swollen stretch λ_0 attached to a rigid substrate.

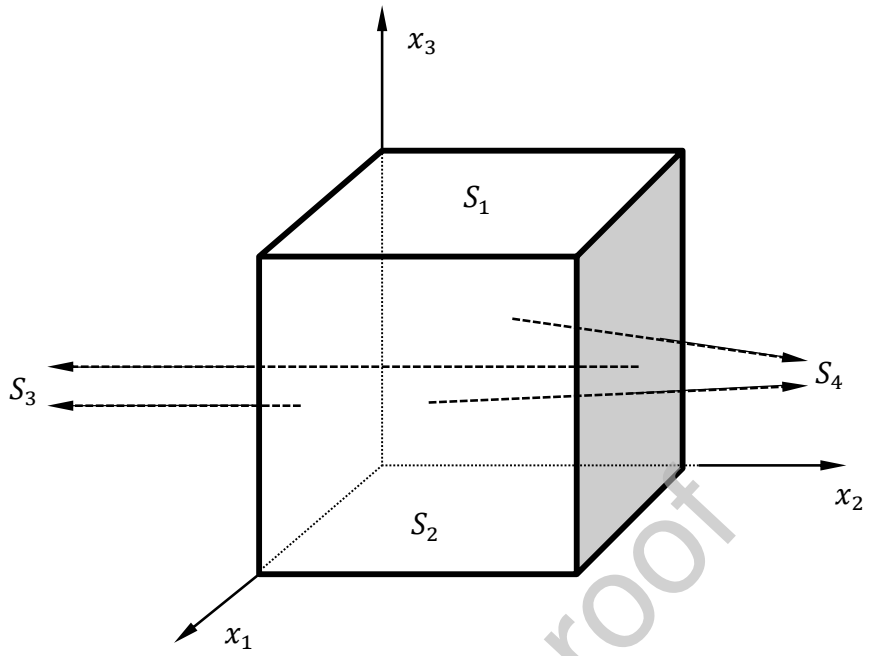

Figure 7 A unit cube of the hydrogel layer. Four kinds of boundary conditions (S_1, S_2, S_3, S_4) are indicated.

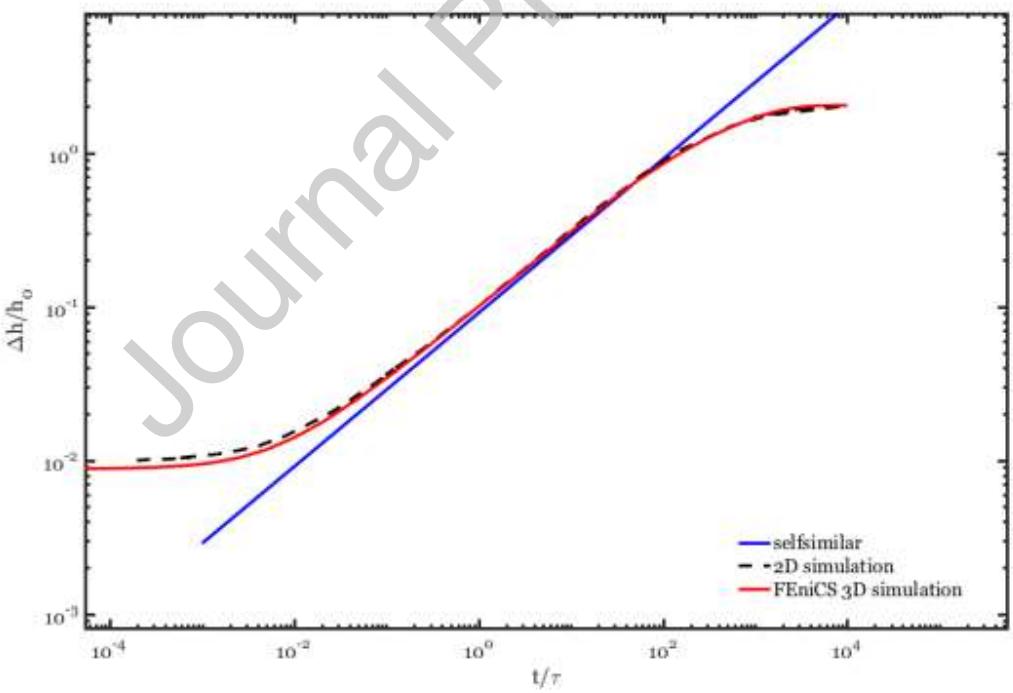

Figure 8. Normalized thickness change during constrained swelling versus the normalized time, comparing the 3D FEniCS model with the 2D finite element model and the self-similar solution in Bouklas et al. (2015).

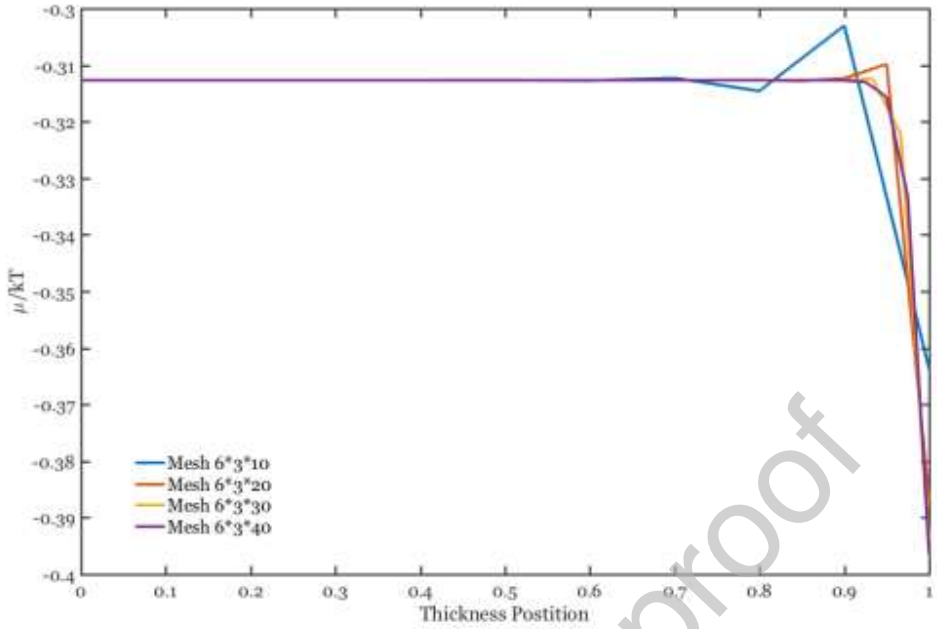

(a)

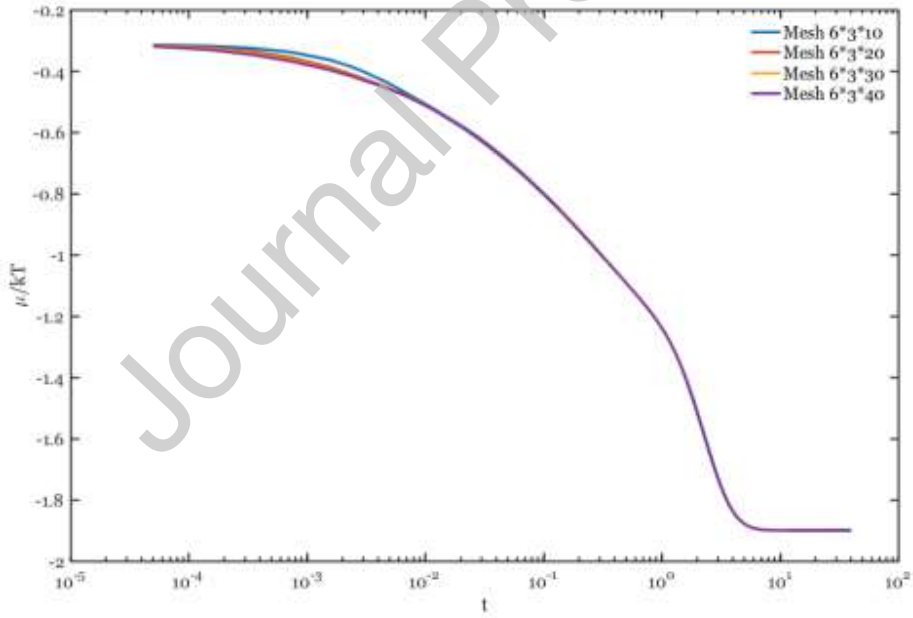

(b)

Figure 9. (a) Variation of the chemical potential along thickness at time 0.0015. (b) Variation of the chemical potential at the point (0,1,0) as a function of time.

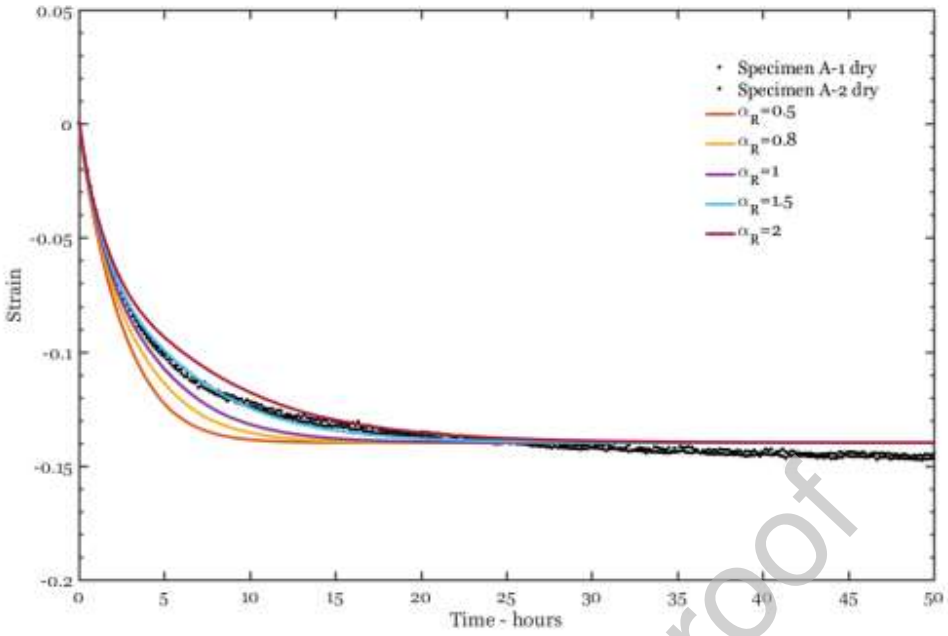

(a)

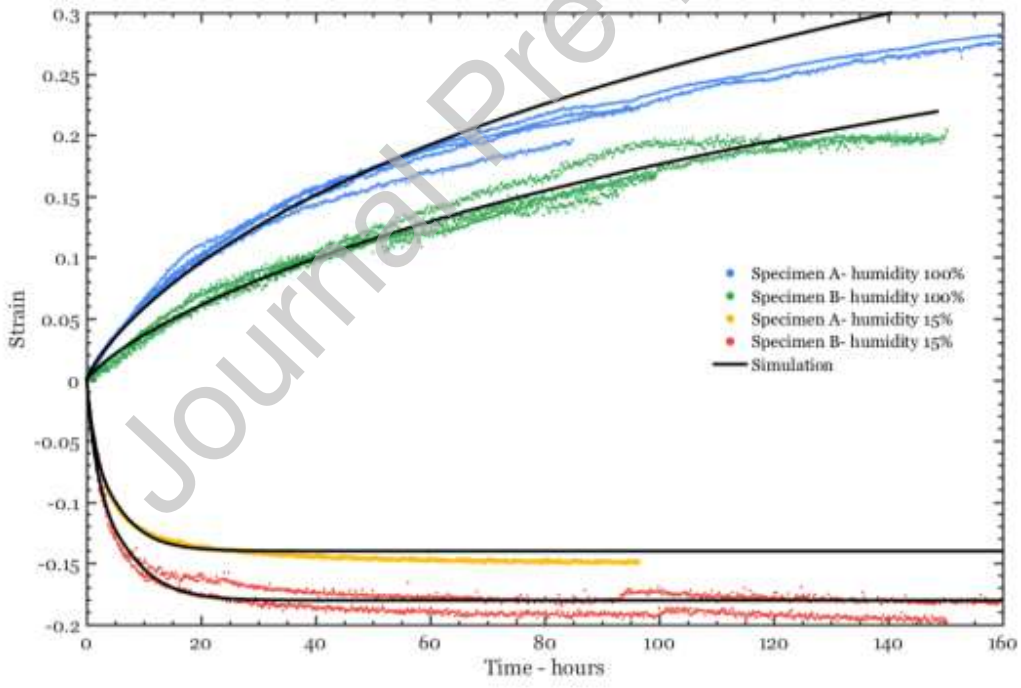

(b)

Figure 10. (a) Comparison of strain versus time between xperiment and simulations for drying test of composition A for different values of α_R with fixed D. (b) Comparison of strain versus time between experiment and simulation for all cases with obtained parameters.

Table 1: Composition of glycerol-water solvent system and gelatin for specimens used.

Composition #	Weight Percent Gelatin	Weight Percent Glycerol	Weight Percent Water
A	15	51	34
B	15	34	51

Table 2:

(a) Material parameters of linear poroelasticity

$\lambda^{\mathrm{dr}} / G$	G / kPa	ν / m^3	$D^* / \left(\mathrm{m}^2\mathrm{s}^{-1}\right)$	α_R
1.6×10^3	33	3×10^{-29}	1.6×10^{-11}	0.66

(b) Material parameters of nonlinear poroelasticity

Specimen	N / m^{-3}	ν / m^3	α_R	$D / \left(\mathrm{m}^2\mathrm{s}^{-1}\right)$	χ	λ_0
A	10^{25}	3×10^{-29}	1.5	8.2×10^{-11}	0.007	1.186
B				7.4×10^{-11}	0.201	1.240

Table 3: Parameters of the linear poroelasticity calculated from the nonlinear poroelasticity

Specimen	G / kPa	ν / m^3	α_R	$\lambda^{\mathrm{dr}} / G$	$D^* / \left(\mathrm{m}^2\mathrm{s}^{-1}\right)$
A	33	3×10^{-29}	1.5	3.5×10^3	3.5×10^{-11}
B				1.9×10^3	2.0×10^{-11}